Eddy current detection of crack orientation using elliptical excitation

T.P. Theodoulidis
S.M. Panas
E.E. Kriezis

Indexing terms: FFT algorithm, Nondestructive testing

Abstract: The use of an elliptical excitation for eddy current detection of crack orientation is investigated. It is shown how the impedance change ΔZ varies as the excitation is rotated above a line crack and how this variation can serve in the detection of the orientation. Numerical results are given for the case of through-thickness line cracks in thin conducting plates. Following the approach of the representation of cracks as a distribution of current sources, attention is concentrated in the evaluation of the field quantities produced by the elliptical excitation in the case of the uncracked thin plate system. The Fourier transformation method is used to treat the differential equations and the fast Fourier transform (FFT) algorithm to perform the calculations.

1 Introduction

During a nondestructive inspection process a quantitative knowledge, relative to the defects that exist in the inspected specimen, is required. In the case of cracks, factors such as the location, shape and orientation have to be determined. This paper is concerned with the evaluation of the orientation's factor by the eddy current NDT method. In the eddy current method a time-varying electromagnetic field is produced by an induction coil causing eddy currents to flow in the inspected conducting specimen. The presence of cracks in the specimen obstructs the eddy current flow and affects coil impedance. The most practical configuration for detecting cracks in a conducting test specimen is by applying an electromagnetic field along the largest dimension of the crack. In this case stronger eddy currents are scattered by the crack and larger impedance change is produced.

Usually, by considering the processing and fabrication history of the specimen to be inspected, some reasonable judgements can be made concerning the possible locations and orientations of cracks that are likely to be present. Then the form of the field to be applied is known beforehand and special shapes of excitation can be used. On the other hand, when no information about the crack characteristics is available, the use of a general-case circular coil makes the detection of the orientation a time consuming practice, the implementation of which gives results only by scanning point by point the entire surface. The use of an elliptical excitation is a practical, alternative choice for the fast detection of the crack orientation as it can produce direction dependent fields. During a plane surface inspection, the excitation located parallel to it can scan the surface without any rotation involved in the procedure until an impedance change occurs indicating the presence of a crack. After the approximate location of the crack has been identified by the previous procedure the excitation can start rotating above the surface to produce a variable field along the crack and thus a variable impedance change. This change is expected to have a minimum and a maximum in amplitude and phase values at certain angles depending on the size of the line crack. After the determination of these angles it is possible then to predict the orientation of the crack by rotating the excitation until only an extremum in the impedance change is detected. By the same procedure, during a tubing or cylindrical bar inspection, the rotation of an internal or encircling elliptical excitation could mark the azimuthal position of a longitudinal crack.

The elliptical excitation was first considered by Panas and Papagiannakis [1]. They studied the case of an elliptical excitation above an infinite slab and the resulting form of the induced eddy currents. The method used here to evaluate the field quantities produced by the elliptical current excitation in the case of the thin plate is the same as in [1]. It involves the Fourier transformation of the differential equations, solution in the spatial frequency domain and inverse transformation of the solution. An important aspect of this method is that it can be applied to any shape of excitation parallel to the plate, once the excitation is expressed in the cartesian system of co-ordinates.

The numerical results presented to show the use of the elliptical excitation are for the case of through-the-thickness straight-line cracks in thin plates. The main approximation of the thin-plate theory is that the thickness of the plate (d) is assumed small compared with the electromagnetic skin depth (δ). The plate is assumed to be nonmagnetic and homogeneous concerning the electrical conductivity, therefore the effects of possible material changes that could occur around cracks cannot be investigated.

The problem of the eddy current flow in thin cracked plates was first considered by Mukherjee *et al.* [2], who

Paper 9582A (S8), first received 10th July 1992 and in revised form 11th March 1993

The authors are with the Aristotle University of Thessaloniki, Department of Electrical Engineering, Thessaloniki, GR 54006, Greece

solved some problems numerically. They observed a singularity in the induced current density at the tips of the cracks as a result of the idealisation of the crack as a perfect geometrical line. Following the formulation of Mukherjee, Hui and Ruina [3] focused their attention at this singularity and found some analytical solutions for a few idealised cases. Later, Burke and Rose introduced a new formalism [4], where the thin conducting plate was represented by an equivalent current sheet and the through the thickness line crack by an equivalent distribution of current sources along the line of the crack. This is followed as it simplifies the problem, in that only the uncracked plate system needs to be considered. The theoretical calculations were found to agree with experiment to within 10% or better for d/δ up to 0.4.

2 Cracks in thin plates

The schematic configuration for eddy-current inspection of a thin conducting plate, containing a through the thickness line crack, and the co-ordinate system is shown in Fig. 1. The plate boundary can be arbitrary, its thickness is d and the conductivity of the plate material is σ. The probe coil induces an eddy current distribution inside the thin plate, assumed to be uniform across the thickness d which is small compared with the electromagnetic skin depth. The thin plate then can be replaced by an equivalent current sheet located at the plane $z = 0$. The line crack has the form of an insulating line represented by an arc C.

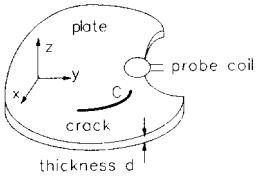

Fig. 1 *Inspection of cracked thin plate*

Assuming excitation with a sine wave at angular frequency ω, Faraday's law in the presence of the current sheet takes the following form

$$\nabla \times \boldsymbol{J}(x, y) = -j\omega\sigma d\boldsymbol{B}(x, y, z = 0) \tag{1}$$

The boundary conditions are

$$[z_0 \cdot \boldsymbol{B}]_{z=0} = 0 \tag{2}$$

$$[z_0 \times \boldsymbol{B}]_{z=0} = \mu_0 \boldsymbol{J}(x, y) \tag{3}$$

where z_0 is the unit vector normal to the thin plate, μ_0 is the magnetic permeability of the plate, the same as that of air, and the square brackets denote the jump across $z = 0$

$$[f]_{z=0} = f(x, y, z \to 0^+) - f(x, y, z \to 0^-) \tag{4}$$

The equivalent surface current density which is divergence free ($\nabla \cdot \boldsymbol{J} = 0$) must be tangential to the crack and the plate boundaries

$$\boldsymbol{J} \cdot \boldsymbol{n} = 0 \tag{5}$$

where $\boldsymbol{n}$ is a unit vector normal to the crack and plate boundaries. Also, the magnetic flux through the crack is zero because it is assumed to have a negligible area in the x–y plane. Use of eqn. 1 and application of Stoke's theorem leads to the following constraint for the circulation of $\boldsymbol{J}$ around the crack

$$\oint_C \boldsymbol{J} \cdot d\boldsymbol{l} = 0 \tag{6}$$

where $\boldsymbol{l}$ is a unit vector tangent to the crack boundary. The equivalent surface current density can be written in the form

$$\boldsymbol{J}(x, y) = \boldsymbol{J}^U(x, y) + \Delta\boldsymbol{J}(x, y) \tag{7}$$

where $\boldsymbol{J}^U$ is the surface current density in the uncracked plate and $\Delta\boldsymbol{J}(x, y)$ is the perturbation due to the crack. Substitution of eqn. 7 in the boundary condition (eqn. 5) results in

$$\Delta\boldsymbol{J} \cdot \boldsymbol{n} = -\boldsymbol{J}^U \cdot \boldsymbol{n} \tag{8}$$

Both $\boldsymbol{J}^U$ and $\Delta\boldsymbol{J}$ satisfy separately eqn. 6, so that, in particular

$$\oint_C \Delta\boldsymbol{J} \cdot d\boldsymbol{l} = 0 \tag{9}$$

The perturbation $\Delta\boldsymbol{J}$ is the contribution of the crack to the surface current density. Thus, the crack can be regarded as an equivalent distribution of sources along the arc C that generate a distribution of generalised current vortices which represent $\Delta\boldsymbol{J}$. A generalised current vortex produced by a source at an arbitrary point (x_0, y_0) is given by the equation

$$\boldsymbol{J}^V(x, y) = \boldsymbol{J}_0^V(x, y) - j\omega\sigma d\boldsymbol{A}^V(x, y, z = 0) \tag{10}$$

where $\boldsymbol{J}_0^V$ is the current density produced by the generalised source and the second term accounts for any currents induced by $\boldsymbol{J}_0^V$, expressed in terms of the corresponding magnetic vector potential $\boldsymbol{A}$, due to Faraday's law. An explicit expression for $\boldsymbol{J}^V(x, y)$ was given in Reference 4 when the plate is the whole plane $z = 0$. The perturbation $\Delta\boldsymbol{J}$ is related to the generalised current vortices via the appropriate vortex density $D(s)$ which can be determined from eqn. 8, which by its turn leads to the following integral equation

$$\int_{crack} dsD(s)\boldsymbol{J}^V(s, s') \cdot \boldsymbol{n}(s') = -\boldsymbol{J}^U(s') \cdot \boldsymbol{n}(s') \quad s, s' \in C \tag{11}$$

where the integral is taken along the arc length of the crack C and $\boldsymbol{J}^V(s, s')$ denotes the generalised current vortex at a point s' along the crack due to a source centred at s. The requirement of eqn. 9 leads to the following constraint for the vortex density.

$$\int_{crack} dsD(s) = 0 \tag{12}$$

3 Impedance change due to a crack

We continue the presentation of the formalism, introduced in Reference 4, by studying the expression of ΔZ in the limit of the thin plate approximation. The impedance change ΔZ due to a crack, which reflects the field distribution around it, is defined as the difference between the coil impedance measured for the cracked plate system Z and the impedance Z^U which would be obtained with an identical but uncracked system, for fixed frequency and coil position relative to the crack. The expression for

ΔZ due to a general flaw in a conductor of arbitrary shape was given by Auld [5]

$$I^2\Delta Z = \int_{S_F} ds \cdot (\boldsymbol{E}^U \times \boldsymbol{H} - \boldsymbol{E} \times \boldsymbol{H}^U) \tag{13}$$

where S_F is an arbitrary closed surface enclosing the flaw but excluding the excitation, ds is the surface element normal to S_F and directed outwards. $\boldsymbol{E}$, $\boldsymbol{H}$ are the fields for the flawed conductor and $\boldsymbol{E}^U$, $\boldsymbol{H}^U$ are the fields for the unflawed conductor. In Reference 4 the simplifications that arise in the case of a line crack in a thin plate were exploited and ΔZ was expressed as the following one-dimensional integral along the crack line

$$I^2\Delta Z = j\omega \int_{crack} dsD(s)W^U(s) \tag{14}$$

which involves the vortex density and the second order magnetic potential W^U [6] when the crack is absent. W^U and $\boldsymbol{J}^U$ are related to the magnetic vector potential for the uncracked plate system via

$$\boldsymbol{J}^U(x, y) = -j\omega\sigma d\boldsymbol{A}^U(x, y, z = 0) \tag{15}$$

and

$$\boldsymbol{A}^U = \nabla \times (z_0 W^U) \tag{16}$$

The result (eqn. 14) is valid for an arbitrary coil configuration. In our work we solve for $W^U(s)$ and $\boldsymbol{J}^U(s)$ for the case shown in Fig. 2. An infinite thin plate with a straight

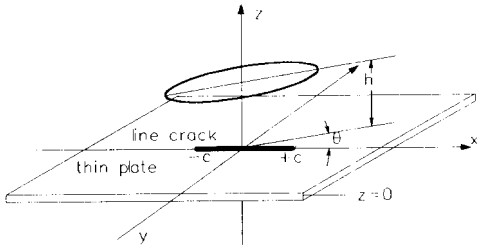

Fig. 2 *Detection of crack orientation by an elliptical excitation: rotation angle is between major axis of ellipse and crack axis*

line crack of length $2c$ in it is considered. The origin of co-ordinates lies at the centre of the crack. A filamentary current excitation of elliptical shape, located parallel to the thin plate is rotated above the line crack. Although the theory given here does not depend on the position of the excitation relative to the crack we will restrict our attention in the special case when the centre of the ellipse lies exactly above the centre of the crack. Thus, only the results of rotation of the excitation are to be considered and interpreted.

The quantities $W^U(s)$ and $\boldsymbol{J}^U(s)$, along the line of the crack, produced by the elliptical excitation, are calculated for rotation angles 0 to 90°. Then, from the solution of eqn. 11 the expression for $D(s)$ is derived and thus, we are able to calculate ΔZ from eqn. 14 as a function of the rotation angle. The analysis with respect to the rotation angle is restricted to the range 0 to 90° because the same impedance change is produced when the excitation is rotated further in multiples of 90°.

For the case of the straight line crack eqns. 11 and 12 take the following form after the normalisation of all lengths by the characteristic crack length c

$$\frac{1}{2\pi}\int_{-1}^{+1} dv \frac{D(v)}{u - v} - \frac{j\beta c}{2\pi}\int_{-1}^{+1} dvD(v)F(u - v) = -J_y^U(cu, 0) \tag{17}$$

where

$$F(v) = \int_0^\infty d\xi \frac{J_1(\xi v)}{\xi + j\beta c} \quad \beta = d/\delta^2 \tag{18}$$

and

$$\int_{-1}^{+1} duD(u) = 0 \tag{19}$$

with $u = x/c$ and $v = x'/c$. J_1 denotes the Bessel function of first kind and first order. Eqn. 17 is a Cauchy-type singular integral equation and because of its widespread occurrence in aerodynamics it is refereed to as 'the generalised airfoil equation'. Together eqns. 17 and 18 define a unique $D(u)$. The specified conditions imply that $D(u)$ is unbounded near $u = \pm 1$ and is proportional to $(1 - u^2)^{-1/2}$ which describes exactly the singularity at the tips of the crack that was observed by Mukherjee *et al.* [2]. The introduction of a new function $D(u) = \Delta(u)(1 - u^2)^{-1/2}$ simplifies matters. Eqns. 17 and 18 then take the form

$$\frac{1}{2\pi}\int_{-1}^{+1} dv \frac{\Delta(v)}{u - v}\frac{1}{\sqrt{(1 - v^2)}} - \frac{j\beta c}{2\pi}\int_{-1}^{+1} dv \frac{\Delta(v)}{\sqrt{(1 - v^2)}} F(u - v) = -J_y^U(cu, 0) \tag{20}$$

and

$$\int_{-1}^{+1} du \frac{\Delta(u)}{\sqrt{(1 - u^2)}} = 0 \tag{21}$$

Eqn. 20 is solved following a method proposed by Erdogan and Gupta in Reference 7 and further justified by Theocaris and Ioakimidis in Reference 8. This method uses the Gauss–Chebyshev quadrature formula

$$\int_{-1}^{+1} \frac{f(t)}{\sqrt{(1 - t^2)}} \simeq \frac{\pi}{n + 1}\sum_{i=0}^{n} f(t_i) \tag{22}$$

where t_i are the roots of the Chebyshev polynomial $T_{n+1}(t)$ for the approximation of eqn. 20. The free variable u is restricted to the values u_j, which are the roots of the modified Chebyshev polynomial $U_n(u)$.

The resulting system of linear algebraic equations supplemented by an additional equation derived from the constraint of eqn. 21, after the use of eqn. 22, provides the values of $\Delta_n(u_i)$ of the approximation $\Delta_n(u)$ at the nodes u_i. Using again the standard Gauss–Chebyshev quadrature formula in eqn. 14, ΔZ can be expressed directly in terms of $\Delta_n(u_i)$. The final result for the impedance change is

$$\Delta Z = \frac{j\omega c}{I^2}\sum_{i=0}^{n} \frac{\pi}{n + 1}\Delta_n(u_i)W^U(cu_i) \tag{23}$$

4 Elliptical excitation

Following the above description of the formalism introduced in Reference 4 for the evaluation of ΔZ due to line

cracks in thin plates, one can calculate W^U and J^U. The procedure followed is to solve for A in the case of the uncracked thin plate system and use eqns. 15 and 16 to obtain expressions for the two quantities of interest. The geometrical configuration of the problem is shown in Fig. 3. A current J_s is flowing in an elliptical loop, situated

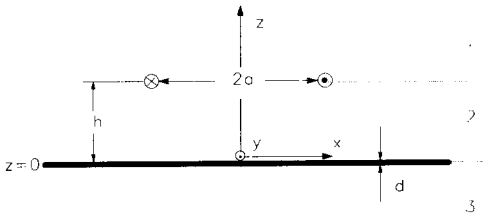

Fig. 3 *Elliptical excitation above thin plate*

parallel and at a distance h above an infinite current sheet of thickness d. The current sheet that represents the thin plate coincides with the x–y plane at $z = 0$. The infinite space is thus divided in three regions. The magnetic vector potential within these regions is a solution of the equation

$$\nabla^2 A_i = 0 \quad i = 1, 2, 3 \tag{24}$$

where a harmonic time dependence of the form $\exp\{+j\omega t)$ is assumed and hereafter suppressed. Since the extent of the conducting medium is infinite along the x–y plane, it follows that the z-component of A_i is zero. Applying the spatial two-dimensional Fourier transform (2D FT) with respect to x and y in eqn. 24 yields, for each Cartesian component of A_i

$$\frac{\partial^2 \hat{A}_{ip}}{\partial^2 z} - k^2 \hat{A}_{ip} = 0 \quad p = x, y \quad i = 1, 2, 3 \tag{25}$$

where $\hat{A}_{ip} = FT_{xy}\{A_{ip}\} = FT_x FT_y\{A_{ip}\}$ and k is the eigenvalue connected to the spatial angular frequency eigenvalues k_x and k_y by the relation $k^2 = k_x^2 + k_y^2$. The circumflex denotes Fourier transformation. The solution of eqn. 25 has the form

$$\hat{A}_{ip} = C_{ip} e^{-kz} + D_{ip} e^{+kz} \tag{26}$$

The appropriate boundary conditions for the computation of the C_{ip} and D_{ip} integration constants are as follows.

(i) The radiation condition for $|z| \to \infty$ which, after transforming and interchanging the order of the limit and integration operators, gives

$$\lim_{|z| \to \infty} \frac{\partial \hat{A}_{ip}}{\partial |z|} + k \hat{A}_{ip} = 0 \quad i = 1, 3 \tag{27}$$

(ii) The boundary conditions eqns. 2 and 3 of the field vectors among the three regions in terms of the Cartesian components of A. After applying a 2D spatial FT, for $z = h$

$$\hat{A}_{1p} = \hat{A}_{2p} \tag{28}$$

$$\frac{\partial \hat{A}_{1p}}{\partial z} - \frac{\partial \hat{A}_{2p}}{\partial z} = -\mu_0 \hat{J}_{sp} \tag{29}$$

for $z = 0$

$$\hat{A}_{2p} = \hat{A}_{3p} \tag{30}$$

$$\frac{\partial \hat{A}_{2p}}{\partial z} - \frac{\partial \hat{A}_{3p}}{\partial z} = 2j\beta \hat{A}_{3p} \tag{31}$$

where $\hat{J}_s$ denotes the 2D spatial FT of the excitation current. Application of the radiation condition to the x and y-components of A in regions I and III gives

$$D_{1x} = D_{1y} = C_{3x} = C_{3y} = 0 \tag{32}$$

Application of eqns. 28–31 forms two 4 × 4 uncoupled linear algebraic systems, one for the x- and one for the y-component of A. The solution of these two systems yields, for the integration constants

$$C_{1p} = \frac{\mu_0 \hat{J}_{sp}}{2k} e^{kh}\left(1 - e^{-2kh} \frac{j\beta}{k + j\beta}\right) \tag{33}$$

$$C_{2p} = \frac{\mu_0 \hat{J}_{sp}}{2} \frac{j\beta}{k(k + j\beta)} e^{-kh} \tag{34}$$

$$D_{2p} = \frac{\mu_0 \hat{J}_{sp}}{2k} e^{-kh} \tag{35}$$

$$D_{3p} = \frac{\mu_0 \hat{J}_{sp}}{2(k + j\beta)} e^{-kh} \tag{36}$$

Observing eqns. 26 and 32–36, one can see that the FT of the components of A can be written as

$$\hat{A}_{ip} = H_i \hat{J}_{sp} \quad i = 1, 2, 3 \quad p = x, y \tag{37}$$

where H_i for $i = 1, 2, 3$ is

$$H_1 = \frac{\mu_0}{2k}\left(1 - e^{-2kh} \frac{j\beta}{k + j\beta}\right) e^{-kz} e^{kh} \tag{38}$$

$$H_2 = \frac{\mu_0}{2k} e^{-kh} e^{kz}\left(1 - \frac{j\beta}{k + j\beta} e^{-2kz}\right) \tag{39}$$

and

$$H_3 = \frac{\mu_0}{2(k + j\beta)} e^{-kh} e^{kz} \tag{40}$$

From eqn. 37 it is concluded that the function H_i is the transfer function of a linear system, as shown in Fig. 4,

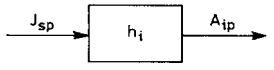

Fig. 4 *Alternative representation of electromagnetic problem*

having the excitation current $\hat{J}_{sp}$ as input and $\hat{A}_{ip}$ as output and where

$$h_i = IFT_{k_x} IFT_{k_y}\{H_i\} \tag{41}$$

and IFT denotes inverse Fourier transformation. To use eqn. 37, the FT of the excitation current has to be evaluated. The complex form of the excitation current can be written as [9]

$$J_s = I\delta_l \boldsymbol{l} \tag{42}$$

where

J_s [A/m^2] = volume current distribution of the excitation
I [A] = magnitude of the line current
δ_l [m^{-2}] = Dirac delta function describing the elliptical curve of the current flow
$\boldsymbol{l}$ = unit vector tangential to the curve of the ellipse and having the direction of the current flow.

As was shown in Reference 1, eqn. 42 reduces to

$$J_s = J_{sx}\mathbf{x}_0 + J_{sy}\mathbf{y}_0 = I\delta_l I = I\delta(z-h)\prod\left(\frac{y}{2b}\right) \times \left\langle -\frac{a}{b}\frac{y}{\sqrt{(b^2-y^2)}}\left\{\delta\left[x-\frac{a}{b}\sqrt{(b^2-y^2)}\right] + \delta\left[x+\frac{a}{b}\sqrt{(b^2-y^2)}\right]\right\}\mathbf{x}_0 + \left\{\delta\left[x-\frac{a}{b}\sqrt{(b^2-y^2)}\right] - \delta\left[x+\frac{a}{b}\sqrt{(b^2-y^2)}\right]\right\}\mathbf{y}_0\right\rangle \quad (43)$$

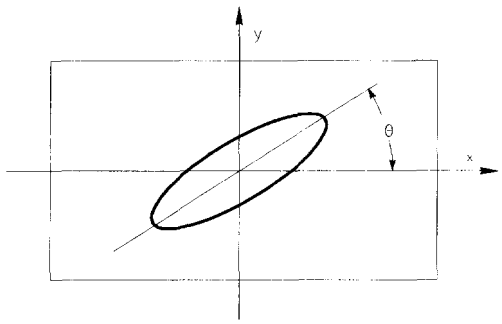

Fig. 5 *Rotation of elliptical excitation*

The 2D FTs of the excitation current density x and y-components take the compact form

$$\hat{J}_{sx} = -jk_y H_0 \quad (44)$$

$$\hat{J}_{sy} = +jk_x H_0 \quad (45)$$

where

$$H_0 = \pi\alpha bI\langle J_0\{\sqrt{[(ak_x)^2 + (bk_y)^2]}\} + J_2\{\sqrt{[(ak_x)^2 + (bk_y)^2]}\}\rangle\delta(z-h) \quad (46)$$

and J_0 and J_2 denote Bessel functions. These results eqns. 44 and 45 are valid only when the major and minor axes of the elliptical excitation are parallel with the x and y co-ordinate axes, respectively. When the excitation is rotated by an angle θ, as shown in Fig. 5, the input $\hat{J}_{sp}$ is changing in contrast to the transfer function H_i which remains invariable and characterises the system.

To calculate $\hat{A}_{ip}$ for the case shown in Fig. 5 J_{sp} has to be modified by the identity of the 2D-FT for the skewed and shifted functions. Given that

$$f(x, y) \xleftrightarrow{\text{2D-FT}} F(\xi, \eta) \quad (47)$$

$$f(a_1x + b_1y + c_1, a_2x + b_2y + c_2) \xleftrightarrow{\text{2D-FT}} \frac{1}{|D|} \times e^{-j2\pi(x_0\xi + y_0\eta)}F\left(\frac{b_2}{D}\xi - \frac{a_2}{D}\eta, -\frac{b_1}{D}\xi + \frac{a_1}{D}\eta\right) \quad (48)$$

where

$$D = a_1b_2 - a_2b_1$$
$$x_0 = (b_1c_2 - b_2c_1)/D$$
$$y_0 = (a_2c_1 - a_1c_2)/D \quad (49)$$

In the case of a simple rotation by an angle θ

$$a_1 = \cos\theta \quad b_1 = \sin\theta \quad a_2 = -\sin\theta \quad b_2 = \cos\theta \quad (50)$$

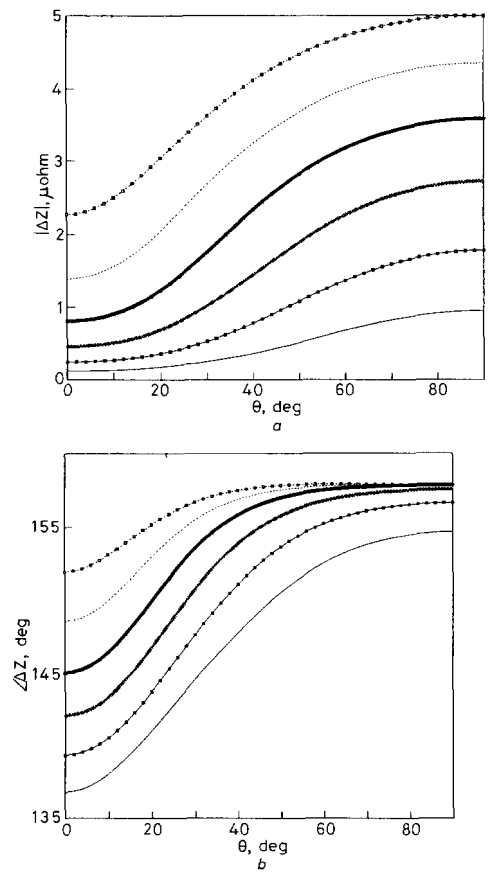

Fig. 6 *Variation of impedance change with rotation angle*

a amplitude
b phase
10 mm = 2c
12 mm = 2c
14 mm = 2c
16 mm = 2c
18 mm = 2c
20 mm = 2c

From eqns. 15 and 16 it is easily verified that the 2D-FTs of the surface current density and the 2D-FTs of the second-order magnetic potential are

$$\hat{J}_x = -j\omega\sigma d\hat{A}_{3x}(z=0) \quad (51)$$

$$\hat{J}_y = +j\omega\sigma d\hat{A}_{3y}(z=0) \quad (52)$$

and

$$+jk_y\hat{W} = \hat{A}_{3x} \quad (53)$$

or

$$-jk_x\hat{W} = \hat{A}_{3y} \quad (54)$$

The inverse FTs of eqns. 51–54, with respect to k_x, k_y give the complex form of the respective field quantities as a function of the x, y-co-ordinates.

The 2D inverse Fourier transform (2D IFT) is performed numerically through the application of the 2D inverse discrete FT (2D IDFT). The evaluation of the 2D

IDFT is made using the two-dimensional inverse fast Fourier transform (2D IFFT) algorithm [10]. There are certain problems arising from the fact that the functions

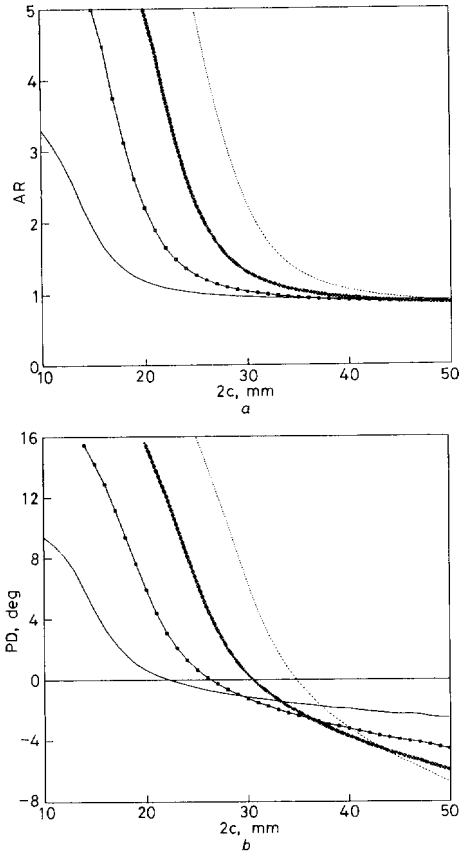

Fig. 7 *Variation of the impedance changes for $\theta = 90°$ and $\theta = 0°$ with crack length*

a ratio between amplitudes
b difference between phases
——— 15 mm = 2*a*
---⊟--- 20 mm = 2*a*
× × × 25 mm = 2*a*
····· 30 mm = 2*a*

to be inverse-transformed are not band limited in k_x and k_y. So a truncation must be done using a rectangular window. The size of the window and the number of samples ($N \times N$) must be chosen so that the aliasing and truncation errors can be minimised.

Another problem is that the values of J and W taken from the 2D IFFT are equidistant in space and the values needed for eqn. 23 are not. An interpolation method has to be applied to calculate these quantities at the roots of the Chebyshev polynomials needed for eqn. 23.

5 Numerical results

The numerical results that are presented are for the case of a nonmagnetic, 1 mm-thick plate of conductivity 1.61×10^7 mho/m (brass). Referring to Figs. 2 and 3 the elliptical excitation current is taken with major axis $2a = 20$ mm and minor axis $2b = 10$ mm. It is located 1 mm above the plate and its frequency is 1 kHz. The ratio d/δ is then 0.25 which agrees with the thin-plate approximation. The line crack lies on the x-axis with its centre below the centre of the ellipse ($|x| \leqslant c$, $y = 0$).

Fig. 6 shows the variation of amplitude $|\Delta Z|$ and phase $\angle \Delta Z$ with the angle of rotation for six crack lengths, $2c = 10$, 12, 14, 16, 18 and 20 mm, which cover the range between the lengths of the major and minor axis of the ellipse. The minimum value in amplitude and phase occurs when the major axis of the ellipse is parallel with the crack and the maximum value when it is perpendicular. That is because for $\theta = 90°$ the excitation is oriented in such a way with respect to the crack that stronger eddy current flow is obstructed.

The longer cracks provide, as expected, larger impedance change both in amplitude and phase. However, the amplitude ratio $AR = |\Delta Z_{90}|/|\Delta Z_{00}|$ and the phase difference $PD = \angle \Delta Z_{90} - \angle \Delta Z_{00}$ becomes smaller as the crack length increases. Thus, although short cracks are harder to detect, the determination of their orientation is easier.

A further investigation examining the effect of crack length to the quantities AR and PD was also performed. Fig. 7 shows their variation related to the crack length, starting from $2c = 10$ mm, for four excitations with a constant minor axis of $2b = 10$ mm and a variable major axis with $2a = 15$, 20, 25, 30 mm. Short cracks provide large AR and PD, therefore only a small a/b is required for the detection of their orientation. For each excitation two critical crack lengths need special attention. The one for which PD is zero and the one for which AR is unity. For the critical length at which the phase does not vary with the rotation the amplitude can be used to detect the orientation. For the critical length at which the amplitude does not vary with the rotation the phase can be used to detect the orientation.

Further increase in the crack length results to an amplitude ratio smaller than unity and a phase difference with negative sign. For very large crack lengths AR grows smaller than unity and PD than zero as the ratio a/b increases. Thus, excitations with increased a/b provide a better detection of the orientation of very long cracks.

6 Conclusions

The previously mentioned results show that the elliptical excitation can be used for the detection of crack orientation as both the amplitude and phase of its impedance vary when it is rotated above a line crack. An important conclusion is that in all cases the two extreme values, the minimum and the maximum, occur when the major axis of the ellipse is parallel or perpendicular to the crack depending on the crack length. Thus, the excitation serves as an azimuthal detector of the crack orientation. Another conclusion is that short cracks, at least shorter than the major axis provide a strong variation in ΔZ as a function of the rotation angle and need excitations with only a small a/b to detect their orientation. On the contrary, long cracks provide a weak variation in ΔZ as a function of the rotation angle and need excitations with increased a/b to detect their orientation.

7 References

1 PANAS, S.M., and PAPAGIANNAKIS, A.G.: 'Eddy currents in an infinite slab due to an elliptic current excitation', *IEEE Trans.*, 1991, **MAG-27**, pp. 4328–4337
2 MUKHERJEE, S., MORJARIA, M.A., and MOON, F.C.: 'Eddy current flows around cracks in thin plates for nondestructive testing', *J. Applied Mechanics*, 1982, **49**, pp. 389–395

3 HUI, C.Y., and RUINA, A.: 'Eddy current flow near cracks in thin plates', *J. Appl. Mech.*, 1985, **52,** pp. 841–846
4 BURKE, S.K., and ROSE, L.R.F.: 'Interaction of induced currents with cracks in thin plates', *Proc. R. Soc. Lond., A*, 1988, **418,** pp. 229–238
5 AULD, B.A.: 'Eddy current characterization of materials and structures'. ASTM Spec. Tech. Publ. 722, 1981, pp. 332–347
6 SMYTHE, W.R.: 'Static and dynamic electricity' (McGraw-Hill, New York, 1968)
7 ERDOGAN, F.K., and GUPTA, G.D.: 'On the numerical solution of singular integral equations', *Q. Appl. Math.*, 1972, **29,** pp. 525–534
8 THEOCARIS, P.S., and IOAKIMIDIS, N.I.: 'Numerical integration methods for the solution of singular integral equations', *Q. Appl. Math.*, 1977, **35,** pp. 173–183
9 PAPOULIS, A.: 'Systems and transforms with applications in optics' (McGraw-Hill, New York, 1968)
10 DUDGEON, D.E., and MERSERAU, R.M.: 'Multidimensional digital signal processing' (Prentice–Hall, 1984)